

## **General Disclaimer**

### **One or more of the Following Statements may affect this Document**

- This document has been reproduced from the best copy furnished by the organizational source. It is being released in the interest of making available as much information as possible.
- This document may contain data, which exceeds the sheet parameters. It was furnished in this condition by the organizational source and is the best copy available.
- This document may contain tone-on-tone or color graphs, charts and/or pictures, which have been reproduced in black and white.
- This document is paginated as submitted by the original source.
- Portions of this document are not fully legible due to the historical nature of some of the material. However, it is the best reproduction available from the original submission.

# Experimental Results of a Deflected Thrust V/STOL Nozzle Research Program

(NASA-TM-83069) EXPERIMENTAL RESULTS OF A  
DEFLECTED THRUST V/STOL NOZZLE RESEARCH  
PROGRAM (NASA) 26 p HC A03/MF A01 CSCL 01A

N83-25657

Unclas

G3/02 03771

Paul L. Burstadt and Albert L. Johns  
*Lewis Research Center*  
*Cleveland, Ohio*

Prepared for the  
Twenty-First Aerospace Sciences Conference  
sponsored by the American Institute of  
Aeronautics and Astronautics  
Reno, Nevada, January 10-13, 1983

Experimental Results of a Deflected Thrust V/STOL Nozzle  
Research Program

Paul L. Burstadt\*  
and  
Albert L. Johns\*

National Aeronautics and Space Administration  
Lewis Research Center  
Cleveland, OH 44135

SUMMARY

Results are presented for an experimental study of four deflected thrust nozzle concepts, designed to operate at the low pressure ratio typical of high bypass-ratio turbofan engines for medium speed (subsonic) V/STOL aircraft. Maps of overall performance characteristics and exit velocity distributions are used to highlight similarities and differences between the four concepts. Analytically determined secondary flows at the exit of a 90° circular pipe bend are compared with the experimental results from the more complex three dimensional geometries. The relative impact of total-pressure losses and secondary flows on nozzle thrust coefficient is addressed by numerical integration of exit velocity measurements.

SYMBOLS

$A_E$	nozzle exit area
$A_0$	nozzle entrance area
alpha	flow angle in plane normal to survey rake
beta	flow angle in plane of the survey rake
CD	discharge coefficient: area required for isentropic expansion of actual flow/ $A_E$
CFN	gross thrust coefficient: $F_N/F_{IDEAL}$
$D_0$	nozzle entrance diameter (33.81 cm.)
$F_{IDEAL}$	thrust of measured mass flow exhausting at $V_{IDEAL}$
$F_N$	measured thrust (kg.)
NPR	nozzle pressure ratio=averaged nozzle entrance total pressure/ambient pressure
$P_t$	total pressure
$P_1, P_2$	pressures from flow angularity probes
$T_t$	total temperature

---

\*Aerospace engineers.

**ORIGINAL CONTAINS  
COLOR ILLUSTRATIONS**

V	velocity as fraction of $V_{IDEAL}$
$V_{IDEAL}$	Velocity after isentropic expansion from average nozzle entrance conditions to ambient conditions
W7SPC	nozzle entrance flow corrected to standard conditions/nozzle entrance area: specific corrected airflow ( $\text{kg./cm.}^2\text{-sec.}$ )
X,Y,Z	horizontal, transverse and vertical axes

## INTRODUCTION

The propulsion systems proposed for medium speed (subsonic) V/STOL aircraft can be categorized as either "fixed nacelle" or "tilt nacelle" systems. When vertical thrust is produced by tilting the nacelle, inlet aerodynamics are a primary concern. However, when the nacelle is fixed, aerodynamics of the thrust deflecting nozzle are a principal topic of study. Four fixed nacelle, medium speed, V/STOL aircraft concepts are shown in figure 1. Fixed nacelle V/STOL aircraft require propulsion system nozzles which can provide high thrust coefficients and efficient flow turning over a wide range of operating conditions. This paper presents the results of an experimental study of the four deflected thrust nozzle concepts utilized by the propulsion systems shown in figure 2. These exhaust systems are designed to operate at the low pressure ratios typical of the high bypass turbofan engines most suited for subsonic V/STOL aircraft.

The NASA-Lewis Research Center's program to study deflected thrust V/STOL nozzles has concentrated on these four configurations which are representative of the broad range that have been proposed. Models shown in figure 3 were obtained under contracts with airframe companies. They were designed for testing with a 30.5cm (12 in) diameter fan and an independently controlled core engine flow simulator. Nozzle performance data were obtained for many variations of each configuration. In addition, a flow survey rake was used to map the velocity components, total pressure and total temperature at the exit of the nozzle.

In general, previous experimental investigations, (references 1-7), have been limited to measurement of conventional nozzle performance coefficients. However, when the nozzle airflow is turned, secondary flows can be generated in the duct, (references 9-14), which represent momentum that is not oriented in a useful direction. Hence, exit velocity distributions are required in order to assess the effect of these rotational flows on nozzle performance. The assessment of the effect of secondary flows on nozzle performance was a primary objective of this research program.

## APPARATUS AND PROCEDURE

### DESCRIPTION OF MODELS

Referring to figure 3a, the "D"-vented nozzle configuration consists of a fixed hood, two rotating hoods, a venting lip, and a core nozzle. The fixed hood is an asymmetric contoured component in which the fan duct transitions from the circular annulus just ahead of the nozzle entrance station, to

a "D" shaped cross section. In the deflecting mode the flow turning process for both fan and core flow is completed in the 'D'-shaped rotating hoods.

The tandem-fan front nozzle of figure 3b consists of an S-duct nozzle and a fairing to cover the base of the fan hub. Both the nozzle wall and the fairing transition vary rapidly from circular to rectangular cross-sections. The lower wall of the S-duct is a two-piece hinged flap, which is rotated to deflect the nozzle flow for V/STOL operation. This nozzle uses only fan airflow.

The chin nozzle system consists of a contoured centerbody, cowl, cascade vane (chin) nozzle, and aft nozzle as shown in figure 3c. Part of the fan airflow is deflected downward, through the cascade vanes. The remainder of the airflow is discharged further aft. This model hardware was designed to study the chin nozzle performance and flow field, and the centerbody represents the turbofan core engine. The hardware aft of the cascade is used simply to remove part of the fan airflow.

The split-flow flap nozzle system shown in figure 3d consists of both a front and an aft deflecting nozzle for fan airflow. This system has a separate nozzle for core engine flow. At some operating conditions almost 100% of the fan flow is deflected through the front nozzle.

#### TEST APPARATUS AND INSTRUMENTATION

The photo in figure 4 shows the 'D'-vented nozzle installed on the Vertical Thrust Stand at the NASA-Lewis Research Center. An inlet bellmouth supplied air to a 30.5 cm (12 in.) diameter fan, which was driven by a tip turbine. Concentric ducts for the fan and turbine discharge flow, and an independently controlled core flow, connected the fan and the nozzle. The nozzle exhausted upward, past the remotely controlled exit flow survey rake. Figure 5 illustrates the internal ducting arrangement and the location of the rake used to measure nozzle entrance conditions. Forces were measured with a six-component balance and thrust was defined as the vector-sum of the axial and normal components. A more detailed description of this test apparatus may be found in reference 7.

When nozzles which did not require core airflow (figures 3b and 3c) were tested, the core nozzle shroud was replaced with an appropriate closed fairing.

Nozzle exit flow measurements were made with the survey rake, which is shown mounted above the nozzle discharge in figure 4. Details of the rake are presented in figure 6. It consists of 20 total temperature probes and 21 flow angularity probes. The three-tube design of the flow angle probes measures total pressure and the angle in one plane, so the probe orientation alternates across the rake to obtain angles in the "pitch" and "yaw" planes. A more extensive discussion of this specific probe design is given in reference 8. The rake support was attached to the non-metric portion of the thrust stand and allowed the rake to be translated in the vertical and horizontal directions, and rotated in the "pitch" plane.

## TEST PROCEDURE

Nozzle entrance test conditions were set by adjusting the valves which provided hot, high pressure air to the fan tip turbine and the core duct. This enabled the nozzle entrance total pressures of the core and fan streams to be independently controlled. When data were being recorded to define the nozzle thrust vector and flow rate (performance data), the exit flow survey rake was moved to a position well away from the exhaust jet. Performance data were obtained over a range of nozzle pressure ratios that was limited by either the maximum speed or the stall limits of the fan. Force measurements at zero-flow conditions were recorded to determine model weight tares required in the determination of thrust.

Nozzle exit flow field data were obtained by setting the desired operating condition and then incrementally moving the survey rake across the exhaust jet. If necessary, the rotary position of the rake was varied at each location to minimize the angle of the flow with respect to the probes. The nozzle entrance conditions were measured at each rake position to account for minor variations of the desired operating condition.

## PRESENTATION AND ANALYSIS OF EXPERIMENTAL RESULTS

The nozzle thrust coefficient,  $C_{FN}$ , is used as the primary measure of system performance and efficiency. In this program, all tests were conducted at static conditions and  $C_{FN}$  is a gross thrust coefficient determined by the measured thrust and mass-flow rate, and the ideal exit velocity. Since measured mass flow is used in the denominator, this coefficient may be interpreted as the ratio of actual-to-ideal velocity at the nozzle exit. Total pressure, total temperature, mass flow rate and area at the nozzle entrance are used to calculate a specific corrected airflow,  $W_{SPC}$ . These parameters are plotted to produce a nozzle performance map which includes lines of constant nozzle pressure ratio (average entrance total pressure/ambient pressure),  $NPR$ , and the ratio of nozzle exit-to-entrance area,  $AE/AO$ . Examples will be discussed in a later section.

A convergent reference nozzle was used to check results obtained from the test facility. Although this reference nozzle was only able to direct thrust in the axial (undeflected) direction, the check was assumed to be valid for all directions since the same procedures were used to calibrate all components of the force balance. As shown and discussed in reference 7, the convergent reference nozzle results demonstrated the need to correct total pressure measured by the nozzle entrance rake to account for boundary layer buildup in the long duct upstream of the rake station. A number of correction methods were tried which produced equivalent results, and the technique of calculating an average total-pressure from the measured values of static pressure, total-temperature, mass flow rate and area at the nozzle entrance station was selected. This value is slightly lower than the average measured with the nozzle entrance rake, because the rake probes were positioned on a simple area-weighted basis and did not account for the wall boundary layers.

Reference 7 presents results which show that the repeatability of thrust coefficient measurements is approximately  $\pm .005$ . This reference also includes a summary of estimated instrumentation accuracy. It should be noted that errors in determining the relatively low nozzle pressure ratios covered by this program have a very strong influence on thrust coefficient through the calculation of ideal velocity. This can be seen by examining the relationship between pressure ratio and ideal exit velocity, and is shown in figure 7 where the indicated value of NPR is 99% of the actual value. For example, at an actual NPR of 1.2 a 1% error in pressure ratio causes a 2.8% error in ideal velocity.

The procedures used to process the pressure and temperature measurement from the nozzle exit survey rake are shown schematically in figure 8. The flow angularity probes were individually calibrated in a free-jet facility, and the resulting calibration functions were used to determine the total pressure and flow angle (either alpha or beta) at each probe location. Temperatures were measured at positions between the flow angle probes. A Lagrangian interpolation procedure was then used to determine all values ( $T_t$ ,  $P_t$ , alpha, beta) at the location of each flow-angle probe. These values were then used to calculate the magnitude of the velocity vector and its components, assuming static pressure in the jet was equal to ambient pressure. Data from the set of survey rake locations which span the jet are interpolated to produce contour maps of  $P_t$ ,  $T_t$  and velocity magnitudes. Examples will be discussed in a later section.

Secondary velocity vector plots are constructed by drawing vectors from the points of measurement in the plane perpendicular to the mean flow. Examples will be discussed later. These plots provide a pictorial representation of the secondary flows in the exhaust jet. The picture is influenced by the frame of reference which is selected, and coordinate system rotations can be used to move the secondary velocity plane. This can be thought of as a change of viewing angle, and will change the magnitude and direction of the secondary velocity vectors. When absolute velocities are used, coordinate system rotations introduce projections of the primary velocity into the secondary plane which complicates the picture. This problem can be avoided by having the observer travel with some part of the flow to remove the effect of the primary velocity. This is done by defining a relative velocity which is the difference between the absolute velocity and a reference value. In practice, the selection of a reference velocity becomes a trial-and-error process. The best picture of vortex-type secondary flows is obtained when the reference velocity is approximately equal to the absolute velocity at the center of rotation.

The Lagrangian interpolation procedure, which was used to construct maps of the exit flow properties measured by the survey rake, was coupled to a numerical integration procedure. Integration of the exit flow field provides a way of investigating the relative contribution of various velocity components to the total thrust of the nozzle. In general, the procedure is represented by the following expression.

$$Q = \frac{\sum_{i=1 \text{ to } m} [\rho_i v_{n_i} A_i Q_i]}{\sum_{i=1 \text{ to } m} [\rho_i v_{n_i} A_i]}$$

where  $m$  is in the range of 500 to 1000,  $A_i$  = survey plane area/m,  $v_{n_i}$  = velocity component normal to survey plane,  $\rho_i$  = density which varies only due to temperature since static pressure is assumed equal to ambient. Density is nearly constant across the jet except in cases of a hot core flow.  $Q$  then represents the mass-weighted average of any quantity  $Q_i$ , which may be a certain velocity component or perhaps the magnitude of the velocity vector.

## RESULTS AND DISCUSSION

### NOZZLE PERFORMANCE COEFFICIENTS

Nozzle performance is usually summarized in the form of a map which plots thrust or velocity coefficient vs. specific corrected airflow, with lines of constant exit area and lines of constant nozzle pressure ratio superimposed. Figure 9a shows a nozzle performance map of this type for a configuration of the vented - 'D' (figure 3a) thrust deflector. Consider a constant area line on this map. This line is related to the engine operating characteristic of pressure ratio versus flow. In this case, and in general, smaller exit areas produce higher thrust coefficients because the specific corrected flow (i.e., Mach number) at the nozzle entrance is reduced for a given pressure ratio (constant pressure ratio lines slope upward to the left). Of course the engine stall line and/or desired operating line determines the minimum allowable exit area.

However, there is an additional factor to be considered when relating nozzle exit area to engine operation, and it is apparent when dealing with deflected thrust nozzles which use "vented" turns. As described in reference 7, the vented nozzle replaces the solid inner wall of the turn with a free-jet boundary. Flow separation along the inner wall of the turn is no longer a problem because the inner wall has been removed. But the free-jet boundary is free to move so that a fixed geometric exit area does not provide a constant effective exit area over the range of pressure ratios. In other words, the discharge coefficient increases with pressure ratio. Effective exit area increases of 2%-4% across the range of pressure ratios (1.1 to 1.35) have been observed, with the amount depending on nozzle design and configuration. Discharge coefficients for this vented - 'D' configuration are presented in figure 9b. The low values of the coefficient are due to the large geometric area used in the denominator. It is the area between the venting lip and the deflecting hood, and jet contraction takes place downstream of this station.

As mentioned above in reference to figure 9a, smaller exit areas produce higher thrust coefficients. But the absolute thrust at a given pressure ratio may increase, decrease or stay the same. The result depends on the slope of the constant pressure ratio lines in figure 9a. The increase in thrust coefficient must more than offset the decrease in nozzle flow rate if the absolute thrust is to increase. Figure 9c shows the absolute thrust levels corresponding to the thrust coefficient values of figure 9a. In this case the increase in thrust coefficient does not offset the decrease in flow and the small exit area has lower thrust at a given pressure ratio.

The deflected thrust nozzle performance characteristics shown in figures 9a through 9c emphasize some of the problems involved with designing and sizing nozzles for this type of VTOL propulsion system. Active trimming of the nozzle exit area may be desired or required in order to match engine operating characteristics, while the size of the propulsion system depends on the relationship between thrust coefficient, pressure ratio and flow rate (i.e., the thrust produced).

Figure 10 shows performance characteristics for a configuration of the tandem-fan front nozzle (figure 3b). The general trends are similar to those discussed above, but there are some additional factors worth noting. The thrust coefficient data for the large exit area in figure 10a exhibits a sharp decline at high pressure ratios as indicated by the dashed line. This behavior has been observed for other deflecting nozzle designs and configurations studied in this program. It generally occurs at the higher values of specific corrected flow, or nozzle entrance Mach number, and is indicative of a change in the internal flow resulting in higher total pressure losses. Figures 10b. and c. show the discharge coefficient and thrust levels, which display characteristics similar to those discussed for figures 9b, and 9c.

The nozzle performance data presented thus far are representative of results obtained with what might be called "full-flow deflector nozzles." All of the flow which enters the nozzle is deflected downward and the flow path is essentially free of obstructions. Split-flow deflector nozzles, as shown in figures 3c and 3d, divide the fan airflow between a front and an aft nozzle. This variable front/aft flow split provides balance and pitch control during VTOL operation, but the core engine and its ducting act as an obstruction to the flow which is deflected through the front nozzle. Flow obstruction in the front nozzle is most obvious in cases where that nozzle must pass a large percentage of the fan flow. This may be necessary due to aircraft transient control requirements.

The thrust and discharge coefficients for the split-flow nozzles of figures 3c and 3d display characteristics similar to the full flow nozzles. However, an additional parameter must be considered. It is the front/aft flow split, and it may effect the performance coefficients of the individual nozzles and the system as a whole. Performance maps are not presented for these configurations in this paper. Early results from the chin cascade system are presented in reference 6, while results from the split-flow flap system and

the tandem-fan will be published in the near future. However, since the front nozzles are the primary interest of this study, it should be noted that they have thrust coefficients, (CFN), in the range of .87 to .90 when passing a high percentage of the fan airflow.

## SECONDARY FLOWS

The analytical method described in reference 15 was used to generate the static-pressure driven secondary velocity field downstream of a 90° pipe bend, shown in figure 11. Flows of this type in the exit stream of a deflector nozzle may be a factor in the difference between measured and ideal thrust, because they represent momentum that is not oriented in a useful direction. Total-pressure losses between the entrance and exit of the nozzle are the primary cause of less-than-ideal thrust, but the possibility of significant secondary flows was a focus of this nozzle research program.

The pattern of figure 11 shows two counter-rotating secondary flows near the inside of the bend, and a migration of flow along the walls from the outside to the inside of the bend. Supporting experimental results are presented and discussed in reference 14.

Experimental measurements of secondary flows at the exits of the deflector nozzles shown in figure 3 were obtained, and selected examples are presented in figure 12. These patterns have an orientation similar to that of figure 11, with the "inside" of the turn on the right and the "outside" of the turn on the left. The rapid geometric transition between the circular (or annular) entrance plane and the 'D' or rectangular shaped deflecting sections of these nozzles, and the presence of centerbodies in two of the designs, produce flow fields that are more highly three-dimensional and less symmetric than the example in figure 11. As discussed above, these "vented" thrust deflectors do not really have a wall on the inside of the turn, which is an additional factor effecting the static pressure distribution inside the nozzle.

Figure 12a shows the secondary velocity field measured just downstream of the vented-'D' nozzle exit. The 'D' shape of the jet is apparent, although the free-jet boundary originating at the venting lip is curved rather than straight. Flow entered the nozzle from the right and has been deflected out of the plane of the paper. Each arrow represents a measurement in the jet, and the spacing is unavoidably much larger than the computational grid used for the analytical results, especially near the boundaries. The third velocity component, out of the paper, is parallel to the measured thrust vector. If the three velocity components associated with the circled arrow are subtracted from the corresponding components at all points, the resulting picture will represent the secondary flow patterns as seen by a moving observer. This result is represented by figure 12b, which also includes a slight rotation (2 degrees) in the x-z plane to enhance the result. A distinct, vortex-type, secondary flow pattern is now apparent in the lower-right corner, bordering on the edge of the jet. A similar selection of a reference velocity and rotation will produce a similar, counter-rotating, flow in the upper-right corner (not shown).

Data from the tandem-fan front nozzle are shown in figure 12c. In this case the nozzle exit is rectangular, with the flap at left and venting lip at right. A distinct flow pattern similar to figure 12b, along with a counter-rotating companion, can be seen even without moving at some reference velocity.

When a centerbody is present and obstructs flow through the nozzle, the secondary flow patterns appear more complex. Figure 12d. consists of data from the exit of the front split-flow flap nozzle while it was passing 100% of the flow. Figure 12e shows results from the exit of the cascade chin nozzle. The distinctive secondary flow patterns noted above have not been located in these examples.

The secondary flow patterns of figures 12a through 12c display characteristics representative of the analytical results in figure 11. However, the geometric complexity of the designs which produced the experimental results may generate secondary flows by mechanisms which do not exist in a circular pipe. A clear example is provided by an experimental configuration which combines hardware from two different nozzle designs.

The tandem-fan front nozzle contains a fairing used to cover the base of the fan hub (figure 3b). This fairing starts with a circular cross-section, transitions to a two-dimensional shape, and helps turn flow through the nozzle. This fairing was installed in the vented-'D' thrust deflector as a replacement for the core nozzle assembly. Figure 12f shows the secondary flow pattern measured with this configuration. The counter rotating patterns near the right-hand boundary of the jet are present again, but the coordinate system reference velocity and orientation have been selected to emphasize another center of rotation in the lower half of the jet. A similar, mirror image, pattern for the top half of the jet is not shown. The direction of rotation is opposite to that observed near the jet boundary, and is thought to be the result of a tip vortex being shed from the fairing. This did not occur when the fairing was used, as designed, in the tandem-fan front nozzle.

#### NUMERICAL INTEGRATION OF VELOCITY COMPONENTS

The numerical procedure described earlier was used to evaluate the amount of thrust loss associated with secondary flows. This procedure assumed that the static pressure in the exit stream of these low pressure ratio nozzles was equal to the ambient value, but the effect of temperature variation was included.

If the total velocity magnitude,  $V$ , is integrated, the result represents the thrust available if the jet was parallel at all points. The actual thrust is represented by the integrated value of the velocity component in a particular direction,  $V_z$ . The difference between these two integrated values represents the effect of all secondary flows, or lack of parallel flow, within the jet. In none of the cases was this effect very important representing at most 2% of the difference between ideal and actual thrust. Although the measured magnitude of secondary velocities was significant (of the order 10% of  $V_{IDEAL}$ ), the momentum associated with them was not. There are two important

factors which contribute to this result. If a secondary velocity occurs in a region of low streamwise velocity there is not much mass flow associated with it. When the streamwise velocity is high, the secondary velocity must be quite large if it is to make a significant impact on direction or size of the total velocity vector. The second factor means that contour maps of the magnitude of the velocity vector, and the component parallel to the thrust direction, look very similar. Differences between them are apparent only in the low velocity regions.

These results from the integration of the exit flow field do not mean that secondary flows are unimportant. Clearly, if the mechanism which generates a secondary flow also produces a reduced streamwise velocity, thrust has been reduced but the above method will not recognize that fact.

#### NOZZLE EXIT VELOCITY CONTOURS

Contour maps of velocity magnitude are shown in figure 13 for a number of cases, including all that were presented in figure 12. Velocity magnitudes have been ratioed to the ideal exit velocity, which is computed from average nozzle entrance conditions and ambient static pressure. The color scale ranges from nearly zero to a value greater than ideal velocity based on average entrance conditions. The scale is linear with the dark blue and green bands at about the 33% and 66% levels respectively.

Figure 13a shows the velocity contour map at the exit of the vented-'D' thrust deflector corresponding to the secondary velocity plot of figure 12a. The rake survey did not quite cover the jet and the shape of the jet boundary is somewhat distorted (notched) by the contour routine where individual rake probes leave, or enter, the stream. The thrust coefficient for this operating condition is approximately 95% and is characterized by a large region of high velocity, with steep gradients at the edge of the jet. The venting lip is located up inside the deflecting hood and the additional mixing with the ambient air is apparent along this side of the jet. This relatively low velocity region is also the location of the distinct secondary flow patterns of figures 12b.

The contour corresponding to the tandem-fan front nozzle data of figure 12c is shown in figure 13b. This survey was made in a horizontal plane just below the deflector flap and some distance below the venting lip and sidewalls, so mixing is more apparent. Performance level and relative size of the high velocity regions are comparable to figure 13a. Again, the secondary velocity patterns discussed above are located in regions of relatively low velocity.

When the front jet of the split-flow flap nozzle system is surveyed, the general shape of the contour map is similar to that shown in the previous figure. This map is shown in figure 13c and corresponds to the conditions of figure 12a (100% flow through the front nozzle). A comparison of figures 13b and 13c indicates the effect of the centerbody obstruction in the latter flow

field. In figure 13c the survey was made closer to the venting lip and sidewalls so there is less spreading of the colors below dark blue. The centerbody effect appears at the center of the jet as larger regions between dark blue, dark green and orange. For these particular configurations, and operating conditions, the difference in thrust coefficient between figures 13b and 13c is about 8% to 9%, which provides some calibration of the eye for visual integration.

Nozzle entrance Mach number, or specific corrected flow, has a strong impact on performance of a deflected thrust nozzle. When the exit area of the split-flow flap front nozzle in figure 13c. is greatly increased (far off-design) by moving the deflecting flap aft, the velocity contour map of figure 13d is the result. Nozzle pressure ratio is the same (1.3) as in figure 13c, but the entrance Mach number has increased from about .41 to about .47, and the thrust coefficient has decreased by 7%.

When the aft-nozzle of the split-flow flap system is opened to pass about 15% of the fan flow, the front nozzle area is reduced and the map of figure 13c becomes that of figure 13e. The overall performance level has increased but the effect of the centerbody is still apparent since much of the flow must still get around the centerbody.

A centerbody is also present in the chin nozzle split flow system. The exit velocity distribution, very close to the exit of the chin nozzle cascade, is shown in figure 13f. Figure 12e shows the corresponding secondary velocity vectors. The cascade consists of six flow passages, and the high velocity flow is located between the sidewalls and the centerbody in the central passages. About 65% of the total flow has passed through the cascade.

If all of the cascade vanes are removed, retaining the front and aft wall contours, the pattern of figure 13g is obtained. The thrust coefficient has improved a little but the center of thrust has moved aft, and without the cascade vanes the thrust deflection angle is greatly reduced. The effect of the centerbody is more apparent, with the higher velocity flow collected on the sides and in the rear corners. With the cascade vanes removed, there are only two short wall surfaces to turn the flow, and the jet shows the effect of separation (black region) from the forward, or "inner," wall of the turn.

The final velocity contour map, figure 13h, shows results from the mixed hardware configuration (vented-'D' deflector hood of figure 3a and tandem-fan hub fairing of figure 3b) discussed in reference to figure 12f. Low velocity "holes" in the upper and lower sections of the jet correspond to the location of the secondary flows discussed above. This is a clear example of a case where integration of exit velocity components would not indicate a significant loss of thrust coefficient due to secondary flows, but where the mechanism which generated them has strongly affected nozzle performance.

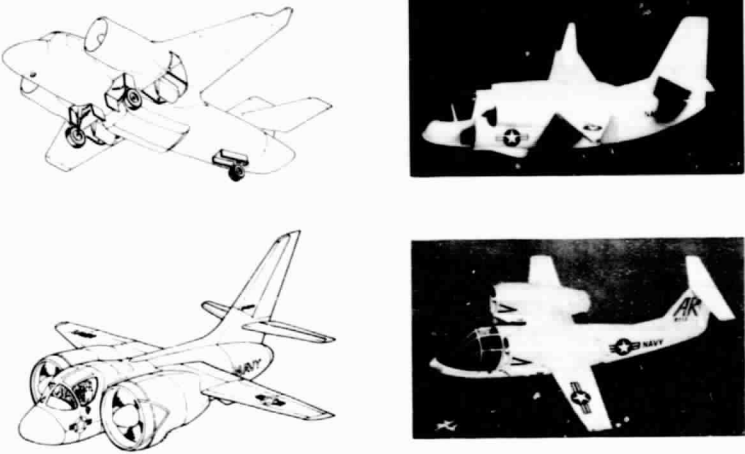
### CONCLUDING REMARKS

1. Deflected thrust nozzle concepts for low pressure ratio, turbofan, propulsion systems have been investigated and shown capable of operating at high levels of thrust coefficient. However, thrust coefficient is very sensitive to small changes in nozzle total pressure loss at these low pressure ratios. Nozzle performance maps reflect this sensitivity in the relationship between performance coefficients, pressure ratio and nozzle entrance Mach number (specific corrected flow), which emphasizes the trade-offs involved when matching a nozzle to this type of V/STOL propulsion system.
2. The V/STOL thrust deflection systems which divide the fan flow between front and aft nozzles displayed lower thrust coefficients than the systems which use a single nozzle to deflect all of the fan flow. The difference is primarily due to the losses involved when flow crosses the centerbody (core engine) to exhaust through the front nozzle. However, it should be noted that the split-flow systems have the capability of varying aircraft pitching moment by changing the front/aft thrust split. The other systems must provide pitching moment control by other means that do not show up specifically as a decrease in nozzle thrust coefficient.
3. Distinct secondary flows were evident at the exit of some of the nozzles and in all cases the magnitude of secondary velocity approached or exceeded 5% of the ideal velocity at some points in the flow. The loss in thrust due to the magnitude of the secondary velocities is was quite small. However, the mechanisms which generate secondary flow do reduce nozzle performance when they also result in reduced streamwise velocities.

## References

1. Limage, C. R., "Development of Low Pressure Ratio Vectoring Nozzles for V/STOL Aircraft," S.A.E. Paper 770988, November 1977.
2. Federspiel, J. F., "Static Test of Large Scale Swivel Nozzle Thrust Deflector," AIAA - 79-1285, June 1979.
3. Esker, D. W., "D Vented Nozzle Thrust Vectoring Performance Tests Using a 10% Scale Dual Flow Model," McDonnell Douglas Report MDC A5703, June 1979.
4. Rosenberg, E. W. and Esker, D. W., "Development of the D Vented Thrust Deflecting Nozzle," AIAA-80-1856, August 1980.
5. Rosenberg, E. W., "Test and Analysis of a Vented 'D' Thrust Deflecting Nozzle on a Turbofan Engine," NASA CR-166279, March 1982.
6. Salemann, Victor, "Static Test of a Fan-Powered 'Chin' Nozzle for V/STOL Applications," NASA CR-165361, April 1981.
7. Watson, T. L., "Tests of a 'D'-Vented Thrust Deflecting Nozzle Behind a Simulated Turbofan Engine," NASA CR-3508, January 1982.
8. Dudzinski, T. J., and Krause, L. N., "Flow-Direction Measurement with Fixed Position Probes", NASA TM X-1904, October 1969.
9. Hawthorne, W. R.: "Secondary Circulation in Fluid Flow," Proceedings of the Royal Society, A206, 1951.
10. Rowe, M., "Measurements and Computations of Flow in Pipes," J. Fluid Mech., 43, 771(1970).
11. Hamed, A., and Abdailah, S., "Three-Dimensional Rotational Flow in Highly Curved Ducts Due to Inlet Vorticity," AIAA - 78-146, 1978.
12. Agrawal, Y., Talbot, L. and Gong, K., "Laser Anemometer Study of Flow Development in Curved Circular Pipes," J. Fluid Mech., 85, 497 (1978).
13. Taylor, A.M.K.P., Whitelaw, J. H., and Yianneskis, M.: "Measurements of Laminar and Turbulent Flow in a Curved Duct with Thin Inlet Boundary Layers," NASA CR-3367, 1981.
14. Enayet, M. M., Gibson, M. M., Taylor, A.M.K.P., and Yianneskis, M., "Laser Doppler Measurements of Laminar and Turbulent Flow in a Pipe Bend," NASA CR-3551, May 1982.
15. Levy, R., McDonald, H., Briley, W. R., and Kreskovsky, J. P.: "A Three-Dimensional Turbulent Compressible Subsonic Duct Flow Analysis for Use with Constructed Coordinate Systems," NASA CR-3389, 1981.

ORIGINAL PAGE  
BLACK AND WHITE PHOTOGRAPH



CS-82-3584

Figure 1. - Medium speed V/STOL aircraft concepts.

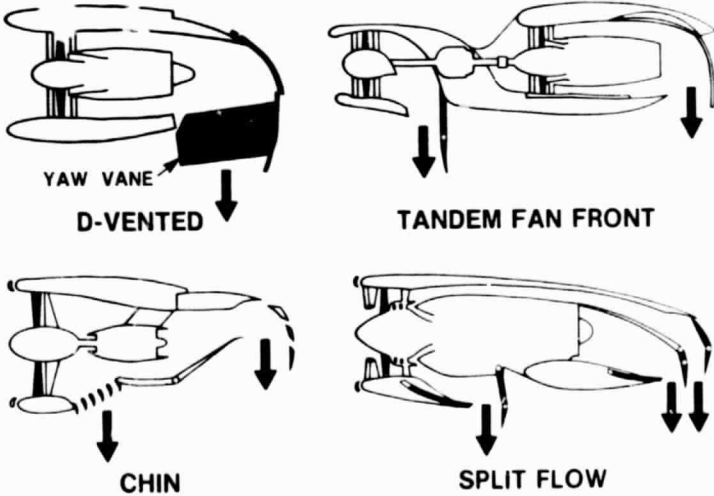
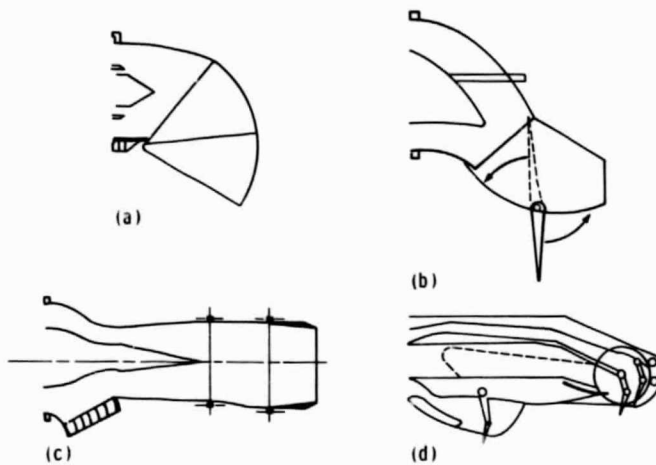


Figure 2. - Medium speed V/STOL propulsion concepts.

ORIGINAL PAGE  
BLACK AND WHITE PHOTOGRAPH



(a) D'-vented (without yaw vane).

(b) Tandem-fan front.

(c) Chin cascade split flow system.

(d) Split flow flap system.

Figure 3. - Experimental models.

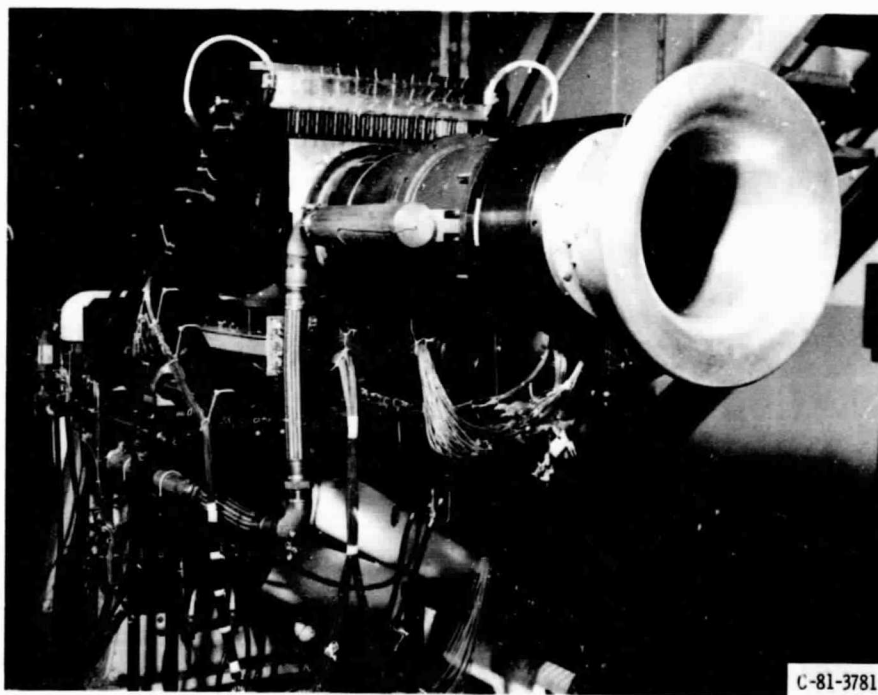


Figure 4. - Test installation with D'-vented nozzle and survey rake.

ORIGINAL PAGE  
BLACK AND WHITE PHOTOGRAPH

ORIGINAL PAGE IS  
OF POOR QUALITY

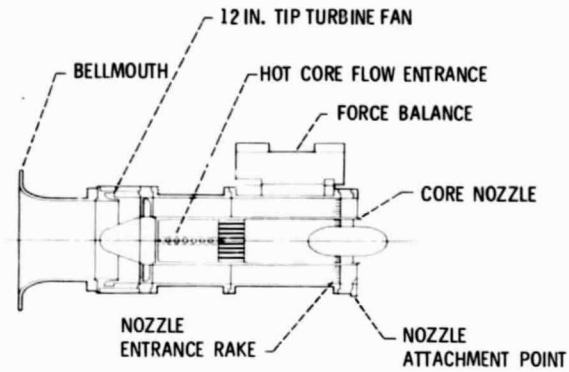


Figure 5. - Schematic of hardware to provide air to test nozzles.

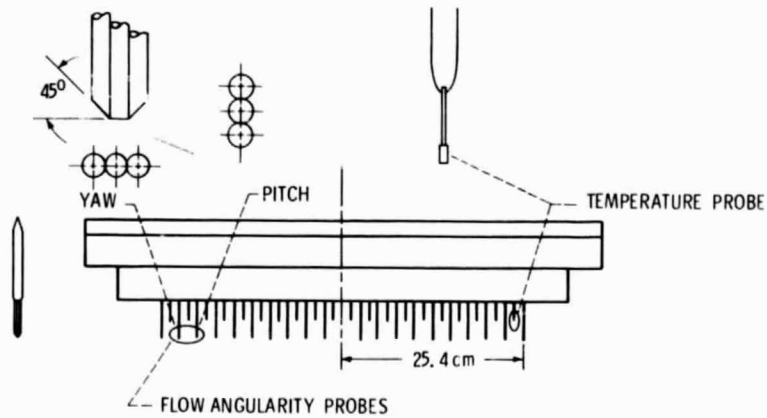


Figure 6. - Details of translating survey rake.

ORIGINAL PAGE IS  
OF POOR QUALITY

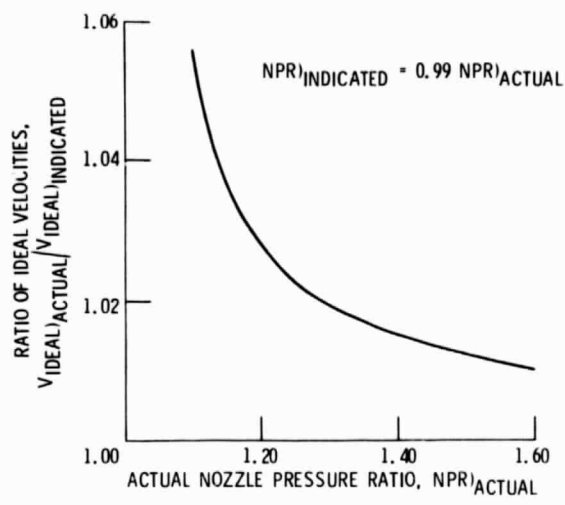


Figure 7. - Sensitivity of ideal velocity to nozzle pressure ratio.

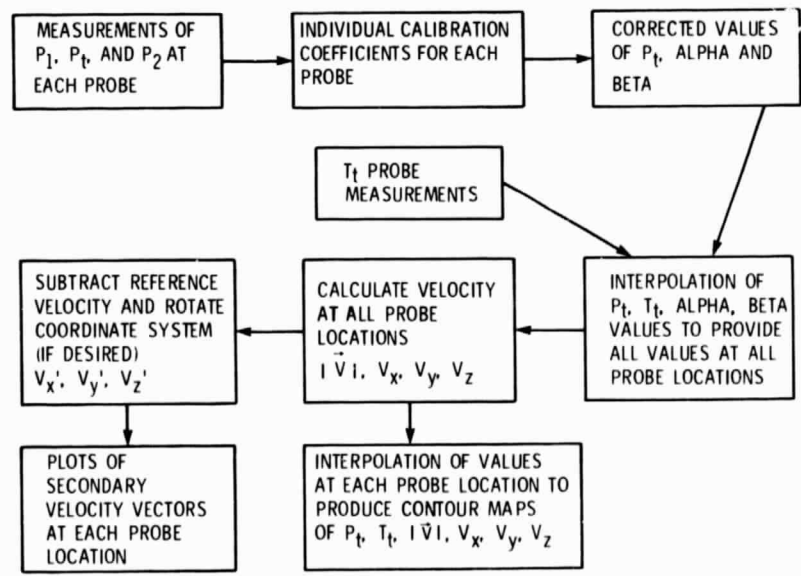
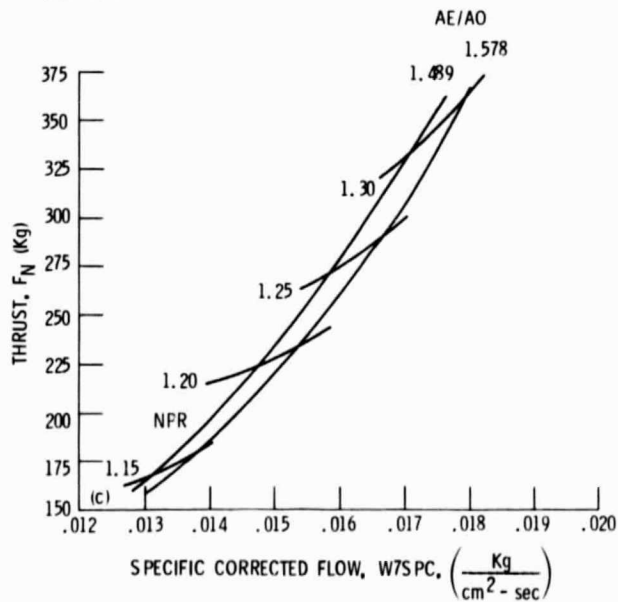
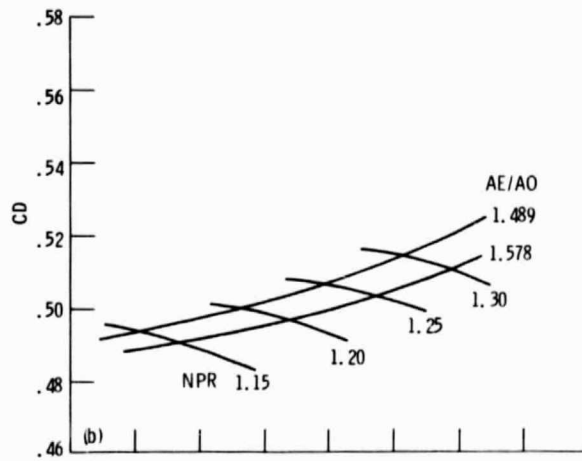
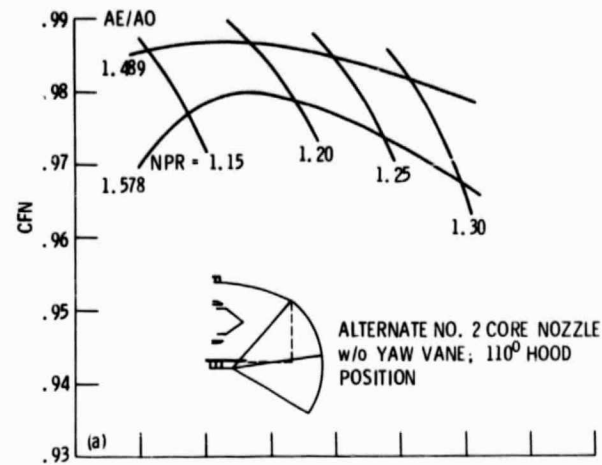


Figure 8. - Data reduction procedure for survey rake measurements.

ORIGINAL PAGE IS  
OF POOR QUALITY

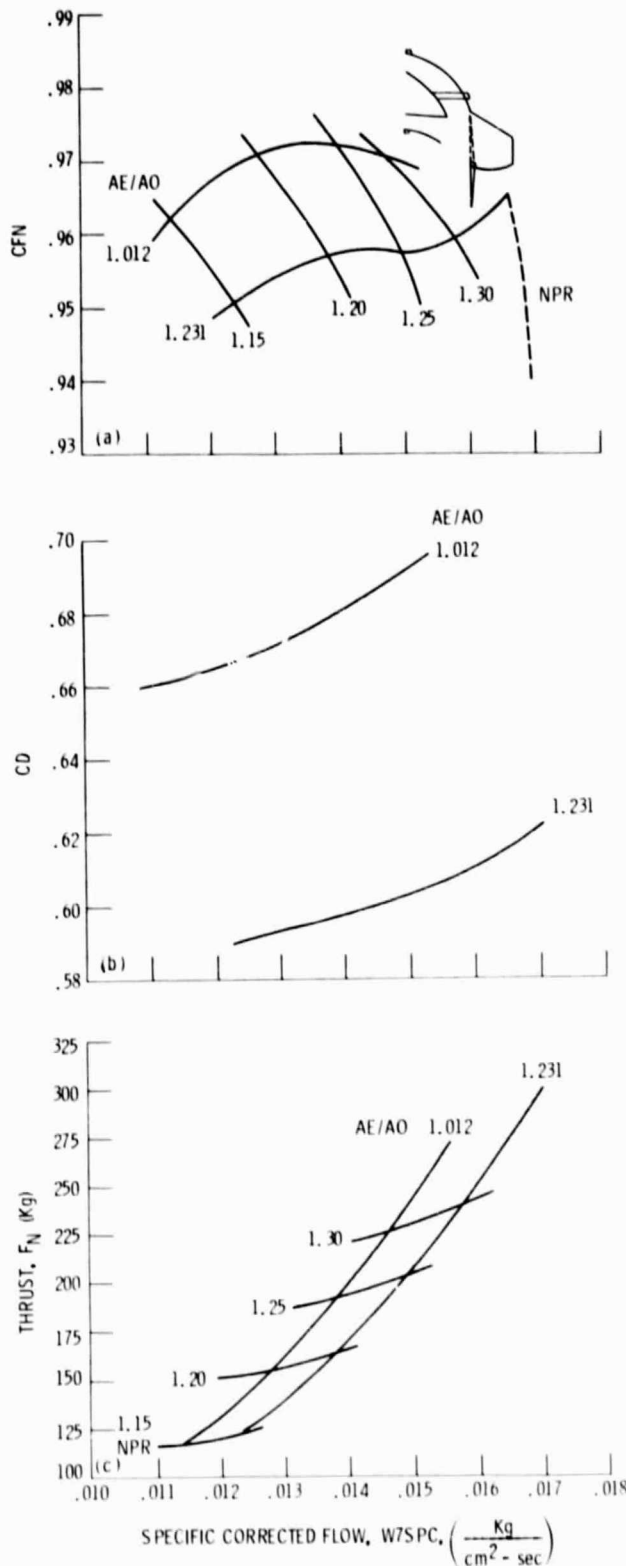
ORIGINAL PAGE IS  
OF POOR QUALITY



- (a) Nozzle thrust coefficient.
- (b) Nozzle discharge coefficient.
- (c) Nozzle gross thrust.

Figure 9. - Nozzle performance for the D-vented nozzle without yaw vane, 110 hood position.

ORIGINAL PAGE IS  
OF POOR QUALITY



- (a) Nozzle thrust coefficient.
- (b) Nozzle discharge coefficient.
- (c) Nozzle gross thrust.

Figure 10. - Nozzle performance for the tandem fan front nozzle.

ORIGINAL PAGE IS  
OF POOR QUALITY

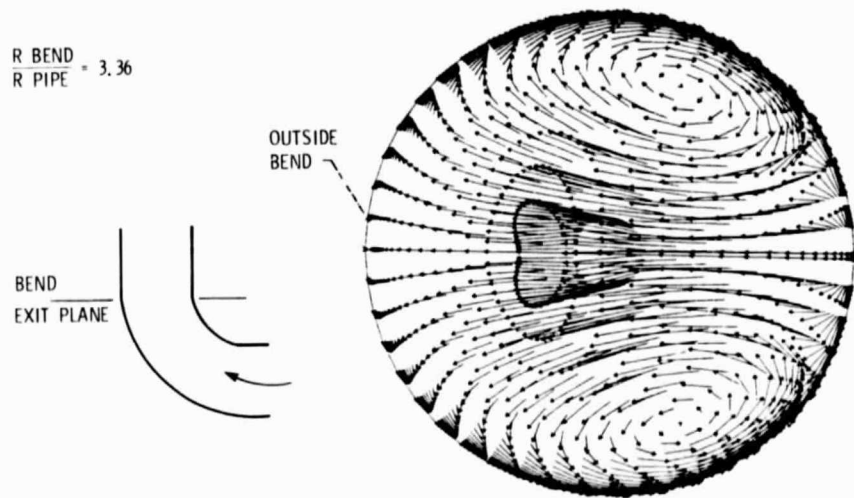
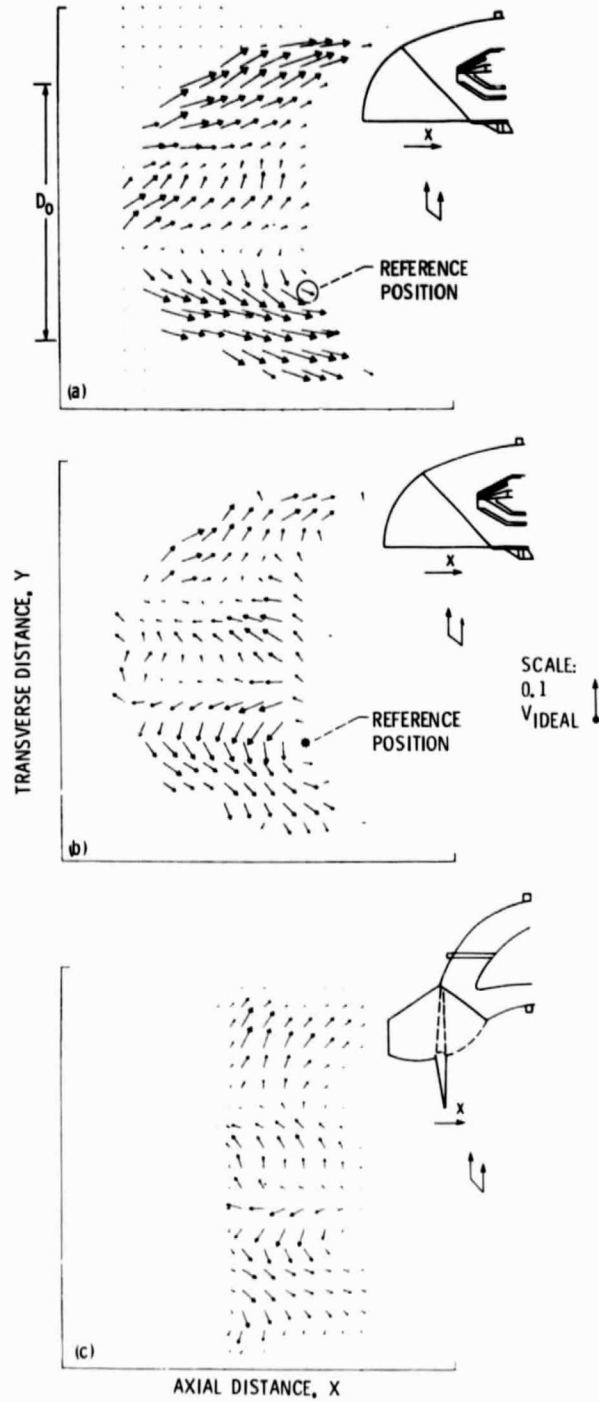


Figure 11. - Secondary flow velocities at exit of a circular pipe bend.

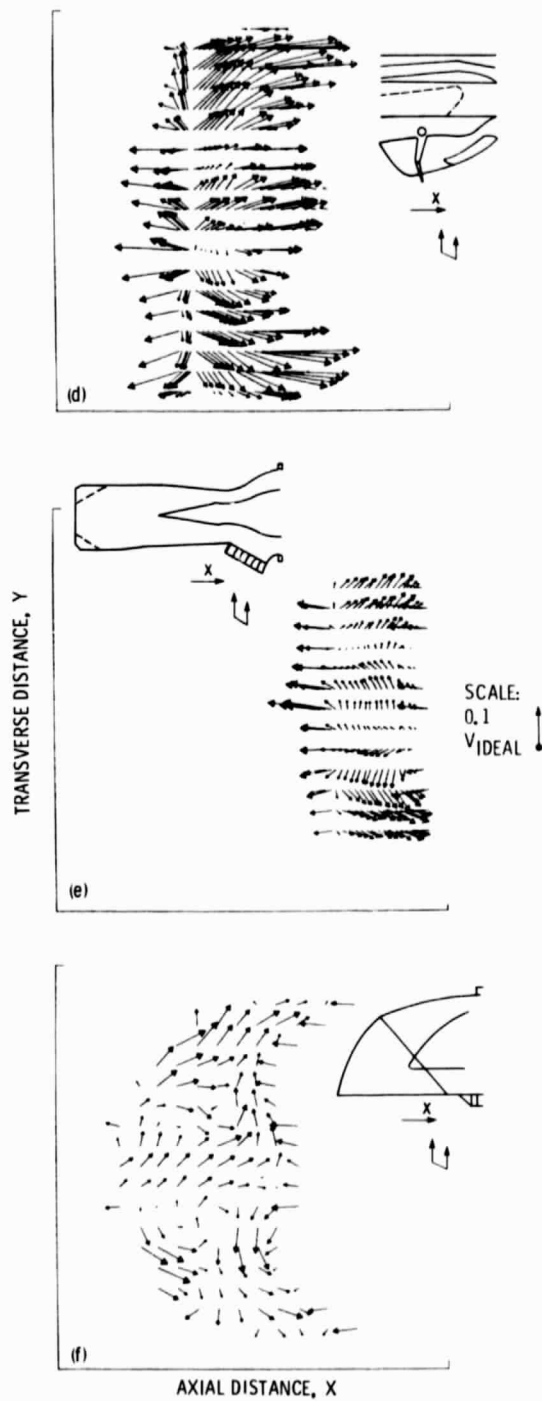
ORIGINAL PAGE IS  
OF POOR QUALITY



(a) 'D'-vented nozzle;  $90^\circ$  hood, core mixer, no yaw vane.  
 (b) 'D'-vented nozzle-reference velocity removed.  
 (c) Tandem-fan front nozzle.

Figure 12. - Secondary velocity vectors at the nozzle exits.

ORIGINAL PAGE IS  
OF POOR QUALITY



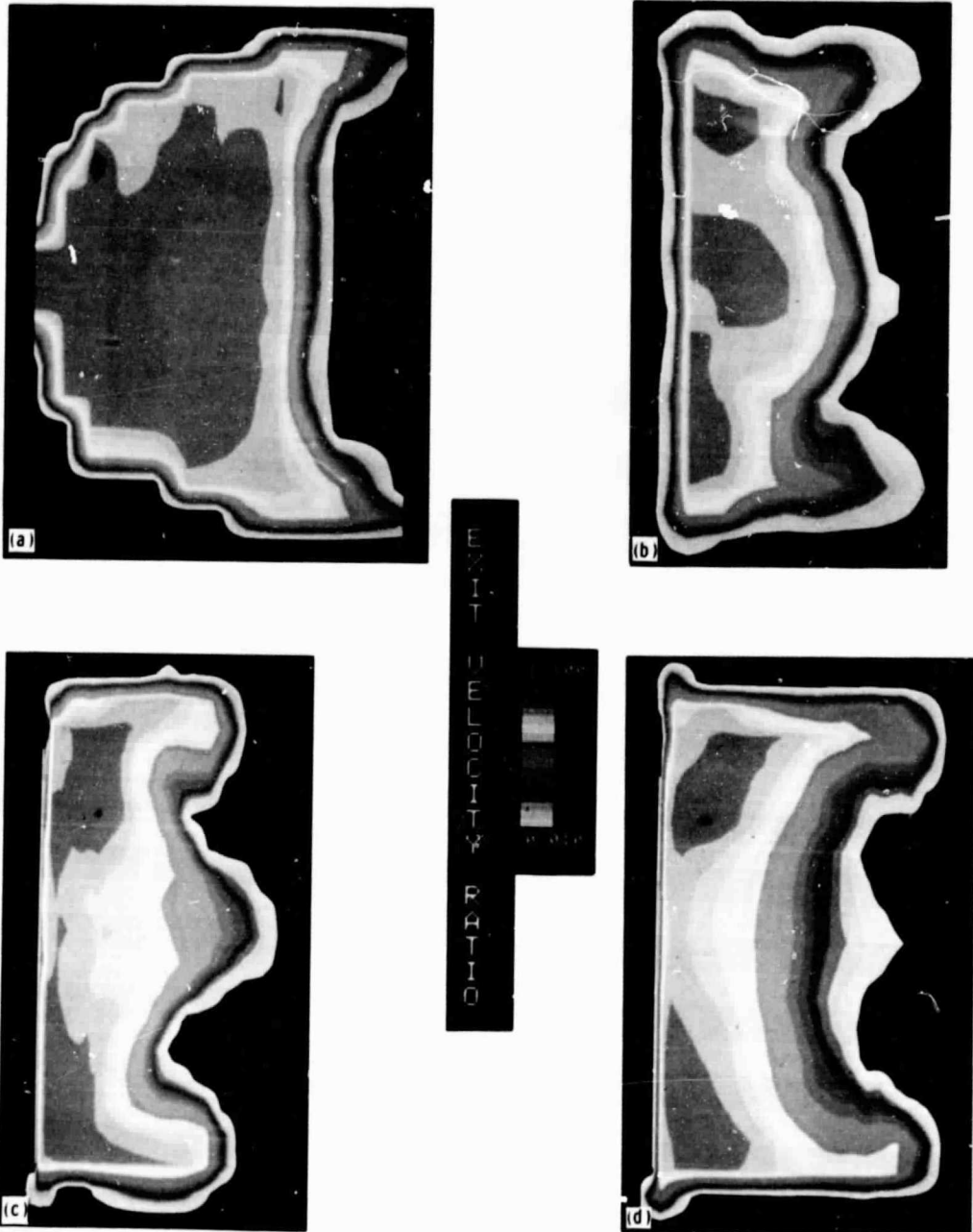
(d) Front nozzle, split-flow flap system: aft nozzle closed.

(e) Chin nozzle with all cascade vanes installed.

(f) 'D'-vented hood and tandem-fan fairing.

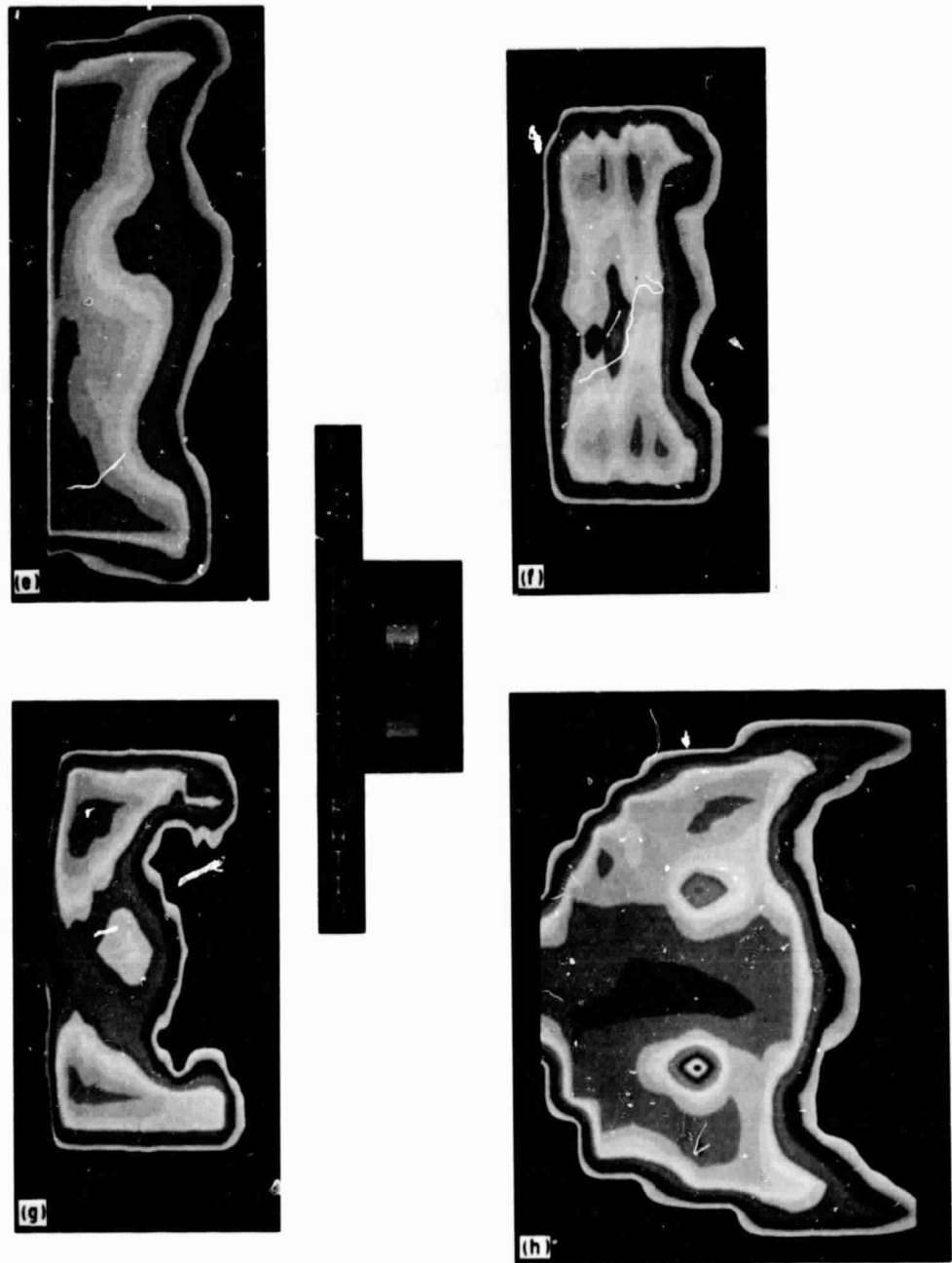
Figure 12. - Concluded.

ORIGINAL PAGE  
COLOR PHOTOGRAPH



(a) 'D'-vented nozzle.  
(b) Tandem-fan front nozzle.  
(c) Split-flow flap, med. front area, aft closed.  
(d) Split-flow flap, large front area, aft closed.  
Figure 13. - Velocity magnitude at nozzle exits.

ORIGINAL PAGE  
COLOR PHOTOGRAPH



- (e) Split-flow flap, small front area; aft open.
- (f) Chin nozzle; cascade vanes installed.
- (g) Chin nozzle; cascade vanes removed.
- (h) 'D'-vented hood and tandem fan fairing.

Figure 13. - Concluded.